



Fast and accurate quantum Monte Carlo for molecular crystals

Andrea Zen^{a,b,c}, Jan Gerit Brandenburg^{a,b,c}, Jiří Klimeš^{d,e}, Alexandre Tkatchenko^f, Dario Alfè^{b,c,g}, and Angelos Michaelides^{a,b,c,1}

^aDepartment of Physics and Astronomy, University College London, London WC1E 6BT, United Kingdom; ^bThomas Young Centre, University College London, London WC1E 6BT, United Kingdom; ^cLondon Centre for Nanotechnology, University College London, London WC1H 0AH, United Kingdom; ^dJ. Heyrovský Institute of Physical Chemistry, Academy of Sciences of the Czech Republic, CZ-18223 Prague 8, Czech Republic; ^eDepartment of Chemical Physics and Optics, Faculty of Mathematics and Physics, Charles University, CZ-12116 Prague 2, Czech Republic; ^fPhysics and Materials Science Research Unit, University of Luxembourg, L-1511 Luxembourg, Luxembourg; and ^gDepartment of Earth Sciences, University College London, London WC1E 6BT, United Kingdom

Edited by Michael L. Klein, Temple University, Philadelphia, PA, and approved January 5, 2018 (received for review September 1, 2017)

Computer simulation plays a central role in modern-day materials science. The utility of a given computational approach depends largely on the balance it provides between accuracy and computational cost. Molecular crystals are a class of materials of great technological importance which are challenging for even the most sophisticated ab initio electronic structure theories to accurately describe. This is partly because they are held together by a balance of weak intermolecular forces but also because the primitive cells of molecular crystals are often substantially larger than those of atomic solids. Here, we demonstrate that diffusion quantum Monte Carlo (DMC) delivers subchemical accuracy for a diverse set of molecular crystals at a surprisingly moderate computational cost. As such, we anticipate that DMC can play an important role in understanding and predicting the properties of a large number of molecular crystals, including those built from relatively large molecules which are far beyond reach of other high-accuracy methods.

quantum Monte Carlo | molecular crystal | electronic structure

Computer simulations, in particular those based on the fundamental laws of quantum mechanics, play a key role in modern materials science research. Such electronic structure approaches serve as an indispensable complement to experiment by helping us understand and predict the properties of materials as well as guiding the development of new ones. Density functional theory (DFT) is the leading electronic structure technique in materials science, thanks to its favorable balance between accuracy and computational cost as well as its efficient implementation in modern codes. Indeed, DFT has been described as one of the great success stories of modern science (1), with widespread use in materials science and cognate disciplines (2–4). However, DFT, as generally applied with standard exchange-correlation functionals, suffers from a number of well-known deficiencies (5–8). One notable shortcoming is in the description of weak interactions such as London dispersion forces. Although the last decade has seen impressive developments with the incorporation of dispersion forces in the DFT framework (9–12), and new density functionals with improved accuracy have been developed (13–15), such approaches are not systematically improvable, and their accuracy for condensed phases is open to question. For example, DFT cannot be relied upon to routinely deliver an accuracy below 4 kJ/mol for the lattice energy of molecular crystals. This is the accuracy (so-called chemical accuracy) that is often needed to discriminate between different polymorphs of a given material, and, in some pharmaceutical molecules, even more stringent accuracies (down to 1 kJ/mol) are needed (16, 17).

Traditionally, highly accurate computations of interaction energies have been based on quantum chemistry techniques, in particular, coupled cluster with single, double, and perturbative triple excitations [CCSD(T)]. However, CCSD(T) calcula-

tions on solids have been notoriously challenging. Great strides forward have recently been made, and CCSD(T) can now be used to study solids through calculations in periodic boundary conditions (18), or by using approaches based on embedding and fragment decomposition (19, 20). The benzene crystal, for example, was recently considered in a tour de force study using fragment decomposition (21). The recent introduction of local approaches (22) promises to extend the range of applicability of CCSD(T) methods. However, the cost of CCSD(T) calculations for large systems will remain high for the foreseeable future, and their large-scale application is additionally hindered by enormous memory requirements. The random phase approximation (RPA) is emerging as a promising approach for materials, in particular if singles corrections are introduced (23–25). Although it is less accurate than CCSD(T), it is considerably more affordable and currently offers a very good balance between accuracy and computational cost. Quantum Monte Carlo, in particular within the fixed node diffusion Monte Carlo (DMC) scheme (26), is an established method for reference quality calculations of molecular systems and condensed phases. Systematic studies in cases of noncovalent bonding have shown that DMC has an accuracy comparable to CCSD(T) (27). An advantage of DMC over traditional quantum chemical methods like CCSD(T) is that it is essentially unaffected by basis set issues, thanks to the deployment of an efficient ground state projection scheme and the

Significance

Computational approaches based on the fundamental laws of quantum mechanics are now integral to almost all materials design initiatives in academia and industry. If computational materials science is genuinely going to deliver on its promises, then an electronic structure method with consistently high accuracy is urgently needed. We show that, thanks to recent algorithmic advances and the strategy developed in our manuscript, quantum Monte Carlo yields extremely accurate predictions for the lattice energies of materials at a surprisingly modest computational cost. It is thus no longer a technique that requires a world-leading computational facility to obtain meaningful results. While we focus on molecular crystals, the significance of our findings extends to all classes of materials.

Author contributions: A.Z., J.G.B., D.A., and A.M. designed research; A.Z., J.G.B., J.K., and D.A. performed research; A.Z., J.G.B., J.K., A.T., D.A., and A.M. analyzed data; and A.Z., J.G.B., and A.M. wrote the paper.

The authors declare no conflict of interest.

This article is a PNAS Direct Submission.

This open access article is distributed under Creative Commons Attribution-NonCommercial-NoDerivatives License 4.0 (CC BY-NC-ND).

¹To whom correspondence should be addressed. Email: angelos.michaelides@ucl.ac.uk.

This article contains supporting information online at www.pnas.org/lookup/suppl/doi:10.1073/pnas.1715434115/-DCSupplemental.

Table 1. Lattice energy (kilojoules per mole) for the molecular crystals under consideration in this work, computed with DMC compared with values from experimental measures of sublimation enthalpy

| Crystal | DMC(lc)* | DMC(sc) [†] | Experiment [‡] |
|--------------------|--------------|----------------------|-------------------------|
| Ice I _h | −59.3 ± 0.5 | −59.2 ± 0.2 | −58.8 |
| Ice II | −59.1 ± 0.6 | −59.0 ± 0.3 | −58.8 |
| Ice VIII | −57.3 ± 0.6 | −57.4 ± 0.1 | −57.4 |
| Carbon dioxide | −28.2 ± 1.3 | −28.5 ± 0.4 | −28.4 |
| Ammonia | −37.1 ± 0.4 | −37.5 ± 0.1 | −37.2 |
| Benzene | −52.1 ± 0.4 | −51.2 ± 0.2 | −50.6 |
| Naphthalene | −78.8 ± 0.8 | −78.0 ± 0.6 | −79.2 |
| Anthracene | −105.5 ± 1.7 | −103.9 ± 1.0 | −105.8 |

*DMC using a large supercell.

[†]DMC using a small supercell; additional values in *SI Appendix*.

[‡]See *SI Appendix, Lattice Energy from Experiments* for details.

actual measure of $\Delta_{\text{sub}}H$ and the computed term $\Delta_{\text{T\&QN}}$ on the order of the chemical accuracy, ~ 4 kJ/mol. For naphthalene and anthracene, which have the largest values for E_{latt} , the experimental uncertainties are likely to be larger. See *SI Appendix* for a detailed discussion on the experimental values. Upon comparing DMC to experiment, we find that both DMC(lc) and DMC(sc) always fall within the accuracy of the experimental value. This is remarkable if we consider that this accuracy is achieved over a large range of lattice energies, E_{latt} from 28 kJ/mol to more than 100 kJ/mol. DMC gets correct lattice energies for hydrogen-bonded, dispersion-bonded and mixed-bonded crystals. DMC also predicts the correct relative energies of the ice polymorphs, yielding slightly improved lattice energies over those reported in ref. 35.

Discussion

A comparison of the results obtained from DMC to experiment and to other reference quality computational approaches is shown in Fig. 2. This includes second order Møller–Plesset perturbation theory (MP2) results for all systems (36–38), and CCSD(T) for all molecules up to benzene (21, 36, 38). RPA and RPA with *GW* singles excitations (RPA+GWSE) lattice energies for ice are calculated in this work, and the other values are from ref. 25. From this comparison, we notice that CCSD(T) and RPA+GWSE perform well, whereas RPA systematically underbinds all systems, and MP2 severely overbinds in systems with delocalized electrons such as benzene, naphthalene, and anthracene. Among the computational approaches reported in Fig. 2, only CCSD(T) is acknowledged for an accuracy comparable to DMC, and, indeed, they show excellent agreement. However, all CCSD(T) (and MP2) values reported come from fragment decomposition approaches, which involve the computation of many small contributions to the lattice energy, all of which must be converged to high accuracy, and, typically, the correlation contribution from long-range fragments is computed at a lower level of theory. This can be a painstaking process. Also the range of values obtained from the widely studied benzene crystal (−50 kJ/mol to −56 kJ/mol) (21, 38–41) suggests that the decisions made in carrying out the fragment decomposition can have a noticeable effect on the final result. A big advantage of methods using periodic boundary conditions, such as DMC, is that the E_{latt} is obtained from a single calculation (provided that FSE are corrected for), which makes such approaches more suitable for rapid screening. As an added bonus, methods such as DMC also yield information on the electronic structure and electron density on the full periodic system, information that can be used for the calculation of experimental observables and to obtain deeper understanding of the system under consideration.

Computational cost is of utmost importance when making comparisons of computational methods. While DMC(lc) and DMC(sc) produce almost equal values for E_{latt} , each DMC(sc) is much cheaper than DMC(lc). For example, as shown in Fig. 2, *Bottom*, DMC(sc) is typically one to two orders of magnitude cheaper. Indeed, most of the DMC(sc) results take around 10^4 CPU hours, and can be obtained in around a day on a few hundred processors. This is much more affordable than CCSD(T), which is also only feasible for relatively small molecules with the fragment decomposition approach or small crystals in periodic boundary conditions. RPA+GWSE has, so far, provided a good compromise between accuracy and computational cost. Fig. 2 shows that the cost for DMC(sc), for a precision on E_{latt} of around 1 kJ/mol, is, in general, comparable to RPA.

The computational efficiency of the DMC simulations and the fact that we have periodic boundary conditions makes it relatively straightforward to investigate other properties beyond the lattice energy. For instance, we have obtained the equation of state (EOS) for both ammonia and benzene; these are crystals held together predominantly by hydrogen bonds and dispersion

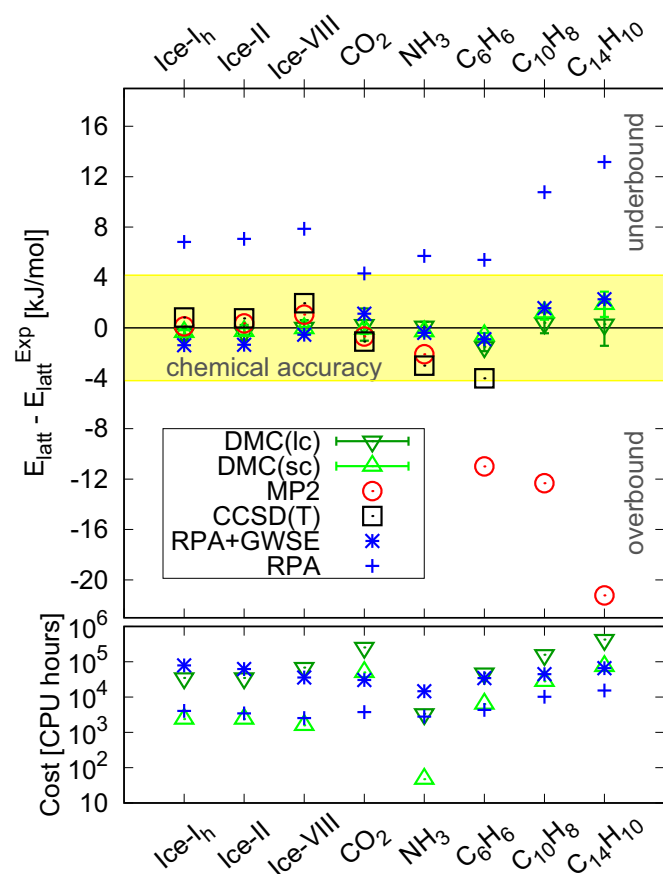


Fig. 2. Accurate and fast DMC results for a range of molecular crystals. (*Top*) Difference in the value of E_{latt} between the experimental value and several computational approaches often used as reference methods. Here DMC(lc) and DMC(sc) indicate that large or small supercells, respectively, have been used. RPA and RPA+GWSE values for ice have been computed in this work; other values are from ref. 25. MP2 and CCSD(T) values for ice are from ref. 36, benzene values are from ref. 21, MP2 values for naphthalene and anthracene are from ref. 37, other values are from ref. 38. (*Bottom*) Approximate computational cost for DMC(sc), DMC(lc), RPA, and RPA+GWSE (see *SI Appendix* for details). The DMC cost is intended for a precision of 0.7 kJ/mol. Reported timings are intended only to provide an indication; differences in the codes and computation facilities can yield very different timings.

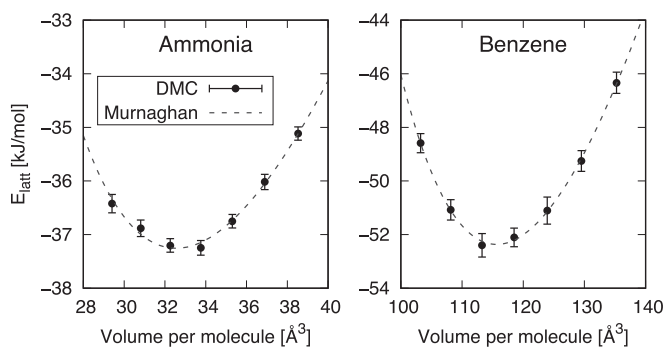


Fig. 3. EOS for the ammonia and benzene crystals (with zero-point motion not accounted for). In both cases, the DMC E_{latt} values are calculated using the $2 \times 2 \times 2$ cell, and FSE are corrected for with MPC. The dashed line is the Murnaghan EOS fitting the DMC values, which, for ammonia, yields a minimum E_0 of -37.25 ± 0.05 kJ/mol at a volume V_0 of 32.6 ± 0.1 Å³ per molecule and a bulk modulus B_0 of 8.5 ± 0.5 GPa; for benzene, E_0 is -52.37 ± 0.06 kJ/mol, V_0 is 115.7 ± 0.1 Å³ per molecule, and B_0 is 7.7 ± 0.2 GPa. The value of B_0 in the Murnaghan EOS is set to 4.

interactions, respectively. The results of these simulations, along with fits to the Murnaghan EOS, are reported in Fig. 3. From this, we find that the equilibrium volumes (V_0) predicted by DMC agree very well with experiment, coming out $\sim 3\%$ smaller than experiment for both crystals. Slightly smaller DMC volumes are to be expected, since our calculations do not take into account anharmonic thermal expansion and quantum nuclear effects present in experiment. The EOS calculations are also useful because they allow us to test the sensitivity of our computed E_{latt} to the volume used in our calculations. The DMC E_{latt} values listed in Table 1 have been obtained at experimentally measured densities. For the two crystals reported in Fig. 3, the bias on E_{latt} arising from the use of the experimental volume appears very small, less than 0.2 kJ/mol. For the other crystals reported in Table 1, we expect, on the basis of DFT tests (25), a bias on E_{latt} due to the volume on the order of 1 kJ/mol or less. A second source of bias on the values of E_{latt} reported in Table 1 is due to the geometries used for the DMC calculations. Indeed, DMC, CCSD(T), MP2, and RPA are typically too expensive for a geometry optimization, which is often performed via DFT with a reliable functional. In *SI Appendix*, we report the EOS of ammonia and benzene obtained using the geometries from two different DFT functionals. The uncertainty on E_{latt} appears to be less than 1 kJ/mol for both ammonia and benzene.

To conclude, we have demonstrated that DMC provides a route toward the fast and accurate determination of the properties of molecular crystals. In essence, the scheme makes use of the size-consistent DMC algorithm introduced earlier (28) and an accurate approach for correcting for FSE. We have applied this approach to a range of exemplar systems held together with a range of intermolecular interactions (hydrogen bonds to London dispersion). The calculations have confirmed previous results on water ice polymorphs but with minimal computational cost and with much more control over the numerical accuracy of the results than before. Our results also include EOS calculations for benzene—the “fruitfly” molecular crystal in computational materials science—and anthracene, the largest molecule in the C21 dataset. The consistently high accuracy demonstrated by DMC, along with its moderate computational cost, suggests that DMC can play an increasingly important role in studies of molecular crystals. In particular, DMC could prove to be the method of choice in challenging polymorph prediction studies. Similarly, molecules of direct pharmaceutical interest could now be tackled with DMC, opening up their

study with a high-level ab initio approach. To provide full phase diagrams for molecular crystals, our accurate lattice energies have to be combined with estimates of zero-point and thermal effects. This is traditionally computed at the DFT level, where our study will further provide an important benchmark to test and calibrate these approximate methods. Looking farther to the future, we note that several steps of the proposed methodology could be used in a full configuration interaction QMC approach (18), which would yield essentially exact solutions to the Schrödinger equation for molecular crystals. Finally, we note that, beyond molecular crystals, the improved efficiencies and improved understanding of FSE obtained here will also be of direct relevance to DMC simulations on other classes of material, e.g., absorption in metal organic frameworks and binding to surfaces.

Materials and Methods

Geometries for the C21 crystals are taken from ref. 25 [where the geometries for molecules and crystals are optimized via DFT using the optB88-vdW functional (42), and crystals are in the experimental unit cell]. For ice phases, we took the geometries used in ref. 35. DMC simulations were carried out with the casino code (43) to evaluate E_{cryst} and E_{gas} . We used Dirac-Fock pseudopotentials (44, 45) with the locality approximation (46). The trial wave functions were of the Slater-Jastrow type with single Slater determinants and the single-particle orbitals obtained from DFT local-density approximation (LDA) plane-wave calculations performed with pwscf (www.quantum-espresso.org/) and reexpanded in terms of B-splines (47). The Jastrow factor included electron-electron, electron-nucleus, and electron-electron-nucleus terms. Further details on the wave function and the optimization are provided in *SI Appendix*, as well as some comparative tests with the recently introduced correlated electron pseudopotentials (48).

In the computation of E_{cryst} , periodic boundary conditions are used. Simulations with DMC in periodic boundary conditions can be subject to significant FSE, as previously discussed. To assess the converged value of E_{latt} , for any molecular crystal, several simulation cells were considered, as well as twist boundary conditions (49) for the smallest cells. This has revealed that

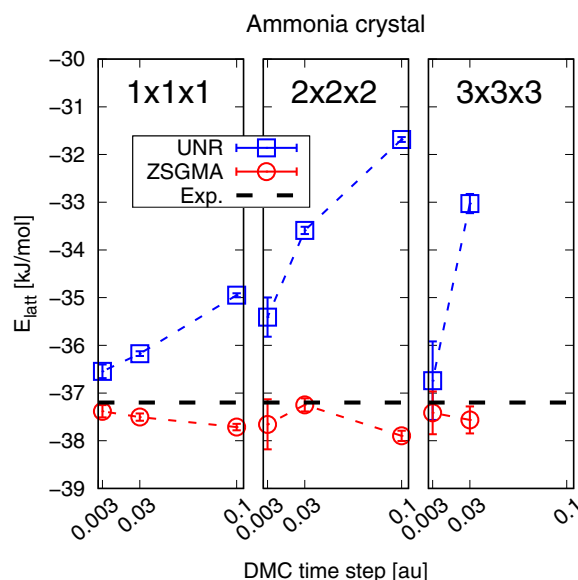


Fig. 4. Converged lattice energies from DMC in small and large unit cells. Lattice energies, E_{latt} , for the ammonia crystal, as obtained from DMC (with the MPC interaction to reduce FSE) by using different time steps and cell sizes, from the primitive $1 \times 1 \times 1$ cell (comprising 4 molecules) to a $3 \times 3 \times 3$ supercell (108 molecules). Blue squares represent the results obtained by using the algorithm by ref. 54 (UNR); red circles correspond to the algorithm by ref. 28 (ZSGMA), which consistently yields accurate results. The black dashed line is the value obtained from experimental sublimation enthalpies by ref. 31 (Exp.).

the E_{latt} obtained from the primitive cell can be overestimated by as much as 300% due to FSE. However, correction schemes to reduce FSE are available in DMC, such as the MPC interaction (29, 50, 51), the correction proposed in ref. 52, and the one in ref. 53. We have tested all of them and observed that MPC provides the best results, as shown in *SI Appendix*. Here we report results obtained exclusively with MPC. A second and smaller source of FSE in DMC stems from the use of single-particle orbitals obtained from a DFT calculation on a single point in the Brillouin zone (typically the Γ -point). This error, called the independent particle finite size error (IPFSE), can be easily estimated and corrected for by performing a few additional DFT calculations. Further computational details are reported in *SI Appendix*, including the atomic coordinates for each molecular system studied.

The time step, τ , is a key issue affecting the accuracy of DMC calculations. In DMC, a propagation according to the imaginary time Schrödinger equation is performed to project out the exact ground state from a trial wave function (26). A time step τ must be chosen, keeping in mind that the efficiency of DMC is directly proportional to τ but the projection is exact only in the continuous limit $\tau \rightarrow 0$. Thus, τ has to be small enough to yield converged results, but as large as possible to make DMC efficient. The time step dependence is system-dependent, so it has to be evaluated on a case-by-case basis. In periodic systems, this can be computationally very expensive, because each supercell is possibly affected by the time step differently. As noted, an improved DMC algorithm (28) was recently presented. The new algorithm, denoted ZSGMA from the authors' initials, gives better convergence with respect to τ than the one proposed by Umrigar, Nightingale, and Runge (UNR) (54) which is implemented as standard in DMC codes. In the evaluation of E_{latt} , an important practical point is the influence of the simulation cell size on the time step error. This is shown in Fig. 4 for the example of the ammonia crystal. Specifically, in Fig. 4, the dependence of E_{latt} on τ is shown for a range of different unit cells. First, it can be seen that, with ZSGMA, E_{latt} exhibits almost no dependence on τ for the range of τ reported. In contrast, values of E_{latt} from UNR show a pronounced and nonlinear dependence on τ . This means that, for UNR simulations, small values of τ (say $\tau \leq 0.001$ au) are required to generate a reliable $\tau \rightarrow 0$ extrapolation. Second, we find that, with ZSGMA, the time step error on E_{latt} is independent of the size of the unit cell (compare the $1 \times 1 \times 1$, the $2 \times 2 \times 2$, and the $3 \times 3 \times 3$ cells in Fig. 4). In contrast with UNR, the time step error increases significantly as the size of the simulation cell is increased. This general behavior can be rationalized by the fact that ZSGMA is (approximately) size-consistent up to relatively large values of τ , while UNR is size-consistent only in the limit $\tau \rightarrow 0$.

In this work, we have verified the time step convergence with the ZSGMA algorithm for each molecular crystal, as reported in *SI Appendix*. It is the larger time step that ZSGMA facilitates and the insensitivity of the time step error to the size of the cell that enable the converged DMC calculations on large crystals reported in this study. All results reported in the work are obtained with the ZSGMA algorithm and a time step that yields a bias of <1 kJ/mol. With the UNR algorithm, the same accuracy would have required difficult extrapolations and a computational cost around two orders of magnitude larger.

We now describe the scheme used here to compute accurate values of E_{latt} with DMC. We recommend the use of the ZSGMA algorithm (28) in all DMC calculations, and the use of MPC for all DMC calculations in periodic systems. The following five-step procedure can be used to assess the lattice energy for a given molecular crystal.

- i) **Geometries** – Obtain geometries for the molecular crystal and the isolated molecule. Since geometry optimizations of large systems are challenging with DMC, we recommend the use of DFT and an exchange-correlation functional that accounts for Van der Waals (vdW) dispersion

forces. If reliable experimental structures are available, the optimization should be performed at the experimental volume.

- ii) **IPFSE** – Using the structure obtained in *i*, converge the energy per molecule in the crystal, $E_{\text{cryst}}^{\text{DFT},\infty}$, using the functional that is used to obtain the single particle orbitals for the DMC calculations (we generally use LDA). Convergence is reached by considering $l \times m \times n$ Monkhorst–Pack grids of increasing size. The difference $E_{\text{cryst}}^{\text{DFT},l \times m \times n} - E_{\text{cryst}}^{\text{DFT},\infty} = \text{IPFSE}_{l \times m \times n}^{\text{DFT}}$ provides a good indication of the independent particle contribution to the FSE in DMC calculations for an $l \times m \times n$ supercell; see *SI Appendix*.
- iii) **Jastrow optimization** – Take the smallest supercell that is compatible with the Jastrow factor (typically the Jastrow factor has cutoffs related to the size of the simulated cell; we suggest using supercells with the maximum radius of a sphere inscribed within the Wigner–Seitz cell of >5 Å) and optimize the Jastrow factor of the quantum Monte Carlo wave function by minimizing the variance (or, alternatively, the variational energy). An optional test of the reliability of the Jastrow can be performed by calculating the DMC binding energy in a molecular dimer extracted from the crystal, and comparing it with a reference value obtained from CCSD(T).
- iv) **DMC time step** – Check the time step dependence either on the cell used in step *iii* or on the molecular dimer.
- v) **Final DMC calculation of E_{latt}** – Take a supercell from step *ii* with the estimation $\text{IPFSE}_{l \times m \times n}^{\text{DFT}}$ smaller than 10 kJ/mol. Perform the DMC simulation for this crystal using MPC, and perform the DMC calculation with open conditions for the molecule. Calculate E_{latt} and correct for the independent particle FSE using $\text{IPFSE}_{l \times m \times n}^{\text{DFT}}$. This yields the final DMC(sc) result. Optionally, consider larger supercells to reduce $\text{IPFSE}_{l \times m \times n}^{\text{DFT}}$ and the MPC correction.

The threshold $\text{IPFSE}_{l \times m \times n}^{\text{DFT}} < 10$ kJ/mol (in step *v*) is motivated by the target accuracy of ~ 1 kJ/mol and a $\sim 10\%$ reliability of the DFT-based IPFSE correction. A more accurate alternative to evaluate the IPFSE is possible (twist averaging) and is discussed in *SI Appendix*.

Supporting Information

SI Appendix provides details of the setup for the DMC, RPA, and RPA+GWSE calculations, a discussion of the FSE, and additional DMC results. In addition, the computational cost of DMC is discussed, as well as of RPA and RPA+GWSE. An extended version of Table 1 is given, and the evaluation of lattice energies from experimental sublimation enthalpies is discussed. Geometries of the molecular crystals and reference molecules used for the DMC, RPA, and RPA-GWSE calculations are given.

ACKNOWLEDGMENTS. A.Z. and A.M. are supported by the European Research Council (ERC) under the European Union's Seventh Framework Program (FP/2007-2013)/ERC Grant Agreement 616121 (Heterolce project). A.Z. and A.M.'s work is also sponsored by the Air Force Office of Scientific Research, Air Force Material Command, US Air Force, under Grant FA8655-12-1-2099. A.M. is also supported by the Royal Society through a Royal Society Wolfson Research Merit Award. J.G.B. acknowledges support by the Alexander von Humboldt Foundation within the Feodor-Lynen program. J.K. is supported by the European Union's Horizon 2020 research and innovation program under Marie Skłodowska-Curie Grant Agreement 658705. We are also grateful, for computational resources, to ARCHER UK National Supercomputing Service, United Kingdom Car–Parrinello (UKCP) consortium (EP/F036884/1), the London Center for Nanotechnology, University College London (UCL) Research Computing, Oak Ridge Leadership Computing Facility (DE-AC05-00OR22725), and IT4Innovations Center of Excellence (CZ.1.05/1.1.00/02.0070 and LM2015070).

1. Burke K (2012) Perspective on density functional theory. *J Chem Phys* 136:150901.
2. Curtarolo S, et al. (2013) The high-throughput highway to computational materials design. *Nat Mat* 12:191–201.
3. Marzari N (2016) The frontiers and the challenges. *Nat Mater* 15:381–382.
4. Sun J, et al. (2016) Accurate first-principles structures and energies of diversely bonded systems from an efficient density functional. *Nat Chem* 8:831–836.
5. Cohen AJ, Mori-Sanchez P, Yang W (2008) Insights into current limitations of density functional theory. *Science* 321:792–794.
6. Peverati R, Truhlar DG (2014) Quest for a universal density functional: The accuracy of density functionals across a broad spectrum of databases in chemistry and physics. *Phil Trans R Soc A* 372:20120476.
7. Medvedev MG, Bushmarinov IS, Sun J, Perdew JP, Lyssenko KA (2017) Density functional theory is straying from the path toward the exact functional. *Science* 355: 49–52.
8. Hammes-Schiffer S (2017) A conundrum for density functional theory. *Science* 355: 28–29.
9. Grimme S, Hansen A, Brandenburg JG, Bannwarth C (2016) Dispersion-corrected mean-field electronic structure methods. *Chem Rev* 116:5105–5154.
10. Klimeš J, Michaelides A (2012) Perspective: Advances and challenges in treating van der Waals dispersion forces in density functional theory. *J Chem Phys* 137: 120901.
11. Beran GJO (2016) Modeling polymorphic molecular crystals with electronic structure theory. *Chem Rev* 116:5567–5613.
12. Hermann J, DiStasio RA, Jr., Tkatchenko A (2017) First-principles models for van der Waals interactions in molecules and materials: Concepts, theory, and applications. *Chem Rev* 117:4714–4758.
13. Sun J, Ruzsinszky A, Perdew JP (2015) Strongly constrained and appropriately normed semilocal density functional. *Phys Rev Lett* 115:036402.

14. Mardirossian N, Head-Gordon M (2014) ω B97X-V: A 10-parameter, range-separated hybrid, generalized gradient approximation density functional with nonlocal correlation, designed by a survival-of-the-fittest strategy. *Phys Chem Chem Phys* 16:9904–9924.
15. Wang Y, Jin X, Yu HS, Truhlar DG, He X (2017) Revised M06-L functional for improved accuracy on chemical reaction barrier heights, noncovalent interactions, and solid-state physics. *Proc Natl Acad Sci USA* 114:8487–8492.
16. Cruz-Cabeza AJ, Reutzel-Edens SM, Bernstein J (2015) Facts and fictions about polymorphism. *Chem Soc Rev* 44:8619–8635.
17. Reilly AM, et al. (2016) Report on the sixth blind test of organic crystal structure prediction methods. *Acta Cryst B* 72:439–459.
18. Booth GH, Grüneis A, Kresse G, Alavi A (2013) Towards an exact description of electronic wavefunctions in real solids. *Nature* 493:365–370.
19. Wen S, Nanda K, Huang Y, Beran GJO (2012) Practical quantum mechanics-based fragment methods for predicting molecular crystal properties. *Phys Chem Chem Phys* 14:7578–7590.
20. Bygrave PJ, Allan NL, Manby FR (2012) The embedded many-body expansion for energetics of molecular crystals. *J Chem Phys* 137:164102.
21. Yang J, et al. (2014) Ab initio determination of the crystalline benzene lattice energy to sub-kilojoule/mole accuracy. *Science* 345:640–643.
22. Werner HJ, Schütz M (2011) An efficient local coupled cluster method for accurate thermochemistry of large systems. *J Chem Phys* 135:144116.
23. Schimka L, et al. (2010) Accurate surface and adsorption energies from many-body perturbation theory. *Nat Mater* 9:741–744.
24. Ren X, Tkatchenko A, Rinke P, Scheffler M (2011) Beyond the random-phase approximation for the electron correlation energy: The importance of single excitations. *Phys Rev Lett* 106:153003.
25. Klimeš J (2016) Lattice energies of molecular solids from the random phase approximation with singles corrections. *J Chem Phys* 145:094506.
26. Foulkes WMC, Mitas L, Needs RJ, Rajagopal G (2001) Quantum Monte Carlo simulations of solids. *Rev Mod Phys* 73:33–83.
27. Dubecký M, Mitas L, Jurečka P (2016) Noncovalent interactions by quantum Monte Carlo. *Chem Rev* 116:5188–5215.
28. Zen A, Sorella S, Gillan MJ, Michaelides A, Alfè D (2016) Boosting the accuracy and speed of quantum Monte Carlo: Size-consistency and time-step. *Phys Rev B* 93:241118(R).
29. Fraser LM, et al. (1996) Finite-size effects and coulomb interactions in quantum Monte Carlo calculations for homogeneous systems with periodic boundary conditions. *Phys Rev B* 53:1814–1832.
30. Beran GJO, Hartman JD, Heit YN (2016) Predicting molecular crystal properties from first principles: Finite-temperature thermochemistry to NMR crystallography. *Acc Chem Res* 49:2501–2508.
31. Reilly AM, Tkatchenko A (2013) Understanding the role of vibrations, exact exchange, and many-body van der Waals interactions in the cohesive properties of molecular crystals. *J Chem Phys* 139:024705.
32. Otero-de-la Roza A, Johnson ER (2012) A benchmark for non-covalent interactions in solids. *J Chem Phys* 137:054103.
33. Price SL, Reutzel-Edens SM (2016) The potential of computed crystal energy landscapes to aid solid-form development. *Drug Discov Today* 21:912–923.
34. Pulido A et al. (2017) Functional materials discovery using energy–structure–function maps. *Nature* 543:657–664.
35. Santra B, et al. (2011) Hydrogen bonds and van der Waals forces in ice at ambient and high pressures. *Phys Rev Lett* 107:185701.
36. Gillan MJ, Alfè D, Bygrave PJ, Taylor CR, Manby FR (2013) Energy benchmarks for water clusters and ice structures from an embedded many-body expansion. *J Chem Phys* 139:114101.
37. Cutini M, et al. (2016) Assessment of different quantum mechanical methods for the prediction of structure and cohesive energy of molecular crystals. *J Chem Theor Comput* 12:3340–3352.
38. Wen S, Beran GJO (2011) Accurate molecular crystal lattice energies from a fragment QM/MM approach with on-the-fly ab initio force field parametrization. *J Chem Theor Comput* 7:3733–3742.
39. Podeszwa R, Rice BM, Szalewicz K (2008) Predicting structure of molecular crystals from first principles. *Phys Rev Lett* 101:115503.
40. Bludský O, Rubeš M, Soldán P (2008) Ab initio investigation of intermolecular interactions in solid benzene. *Phys Rev B* 77:092103.
41. Ringer AL, Sherrill CD (2008) First principles computation of lattice energies of organic solids: The benzene crystal. *Chem Eur J* 14:2542–2547.
42. Klimeš J, Bowler DR, Michaelides A (2010) Chemical accuracy for the van der Waals density functional. *J Phys Cond Mat* 22:022201.
43. Needs RJ, Towler MD, Drummond ND, Rios PL (2010) Continuum variational and diffusion quantum Monte Carlo calculations. *J Phys: Condens Matter* 22:023201.
44. Trail JR, Needs RJ (2005) Norm-conserving Hartree-Fock pseudopotentials and their asymptotic behavior. *J Chem Phys* 122:014112.
45. Trail JR, Needs RJ (2005) Smooth relativistic Hartree-Fock pseudopotentials for H to Ba and Lu to Hg. *J Chem Phys* 122:174109.
46. Mitas L, Shirley EL, Ceperley DM (1991) Nonlocal pseudopotentials and diffusion Monte Carlo. *J Chem Phys* 95:3467–3475.
47. Alfè D, Gillan MJ (2004) Efficient localized basis set for quantum Monte Carlo calculations on condensed matter. *Phys Rev B* 70:161101.
48. Trail JR, Needs RJ (2013) Pseudopotentials for correlated electron systems. *J Chem Phys* 139:014101.
49. Lin C, Zong FH, Ceperley DM (2001) Twist-averaged boundary conditions in continuum quantum Monte Carlo algorithms. *Phys Rev E* 64:016702.
50. Williamson AJ, et al. (1997) Elimination of coulomb finite-size effects in quantum many-body simulations. *Phys Rev B* 55:R4851–R4854.
51. Kent PRC, et al. (1999) Finite-size errors in quantum many-body simulations of extended systems. *Phys Rev B* 59:1917–1929.
52. Chiesa S, Ceperley DM, Martin RM, Holzmann M (2006) Finite-size error in many-body simulations with long-range interactions. *Phys Rev Lett* 97:076404.
53. Kwee H, Zhang S, Krakauer H (2008) Finite-size correction in many-body electronic structure calculations. *Phys Rev Lett* 100:126404.
54. Umrigar CJ, Nightingale MP, Runge KJ (1993) A diffusion Monte Carlo algorithm with very small time-step errors. *J Chem Phys* 99:2865–2890.